Fissionlike events in the $^{14}N + ^{181}Ta$ system

Vijay R. Sharma,[1] R. Kumar,[2,*] S. Mukherjee,[3] E. F. Aguilera,[1] Mohd. Shuaib,[4] Pushpendra P. Singh,[5] Abhishek Yadav,[6] R. Dubey,[7] S. Appannababu,[8] J. C. Morales-Rivera,[1] S. Kumar,[2] B. P. Singh,[4,†] and R. Prasad[4]

[1]*Departamento de Aceleradores, Instituto Nacional de Investigaciones Nucleares, Apartado Postal 18-1027, Codigo Postal 11801 Mexico, Distrito Federal, Mexico*

[2]*NP-Group, Inter-University Accelerator Centre, New Delhi 110 067, India*

[3]*Department of Physics, Maharaja Sayajirao University of Baroda, Vadodara 390 002, India*

[4]*Department of Physics, Accelerator Laboratory, Aligarh Muslim University, Aligarh 202 002, India*

[5]*Department of Physics, Indian Institute of Technology Ropar, Punjab 140 001, India*

[6]*Department of Physics, Jamia Millia Islamia, New Delhi-110025, India*

[7]*iThemba LABS, National Research Foundation, P.O. Box 722, 7129 Somerset West, South Africa*

[8]*Departamento de Fisica Nuclear, Instituto de Fisica, Universidade de Sao Paulo, Código de Endereçamento Postal 05508 090, Brazil*

(Received 2 October 2018; revised manuscript received 18 October 2018; published 25 March 2019)

Absolute cross sections for 22 fissionlike fragments concerning their decay mode via independent and cumulative cross sections have been measured at four projectile energies, i.e., 82.2 ± 0.8, 79.18 ± 0.82, 76.8 ± 1.2, and 72.9 ± 0.91 MeV. The recoil-catcher activation technique followed by offline γ-ray spectrometry was employed. The isotopic yield distribution and the variance for indium isotopes have been obtained from the experimental data and were found to be in agreement with the literature values. The fissionlike fragments mass distribution is found to be a single-peaked Gaussian distribution and confirms their population via deexcitation of the compound nucleus. The mass distribution variance is found to be narrower and exponentially increases as compared to relatively heavier systems at above 20% of the Coulomb barrier. A self-consistent approach for determining the isobaric charge dispersion parameters has been adopted. The present paper suggests that fission is one of the competing modes at low energies other than complete fusion and incomplete fusion processes.

DOI: 10.1103/PhysRevC.99.034617

I. INTRODUCTION

In recent years, much interest has been aroused due to unexpected products observed in the heavy-ion- (HI-) induced reactions at energies below 10 MeV/A. These products were not from the complete fusion (CF) and incomplete fusion (ICF) of HIs but had signatures similar to those of fission fragments [1–5]. In general, at low energies for heavy-ion interactions involving medium to midheavy mass targets the composite system decays via particle evaporation, which always has an important part of the cross section. On the other hand, it has been observed that nuclear reactions characterizing transfer of a large number of nucleons are known as incomplete fusion which may exist at the interface between direct and compound nucleus reactions [6–8]. Depending upon the excitation energy and angular momentum imparted to the system, the compound nucleus (populated via fusion and/or breakup fusion) may tend towards the fission [9,10]. Ordinarily, the fission process offers a great possibility to understand how two nuclei in contact show up their excitation energy and angular momentum. Recently, Schmidt and Jurado [11], presented fission dynamics based on the energy sorting within the frame of statistical arguments, i.e., why the number of emitted neutrons depends on the excitation energy during the fission process. In terms of the angular momentum, evidence for the fissionlike processes in the final stage of the incomplete fusion was first presented by Sikkeland *et al.* [12]. They observed fissionlike events among the heavy ions, such as ^{12}C, ^{14}N, ^{16}O, and ^{20}Ne on medium mass targets. Viola, Jr. and co-workers [13] made an attempt to explore the dynamics of fission events based on linear momentum transfer from the projectile to the target nucleus using the results of fission fragments angular correlation measurements. They estimated that the critical angular momenta derived do not show any major disagreement with the rotating liquid-drop predictions and hence fissionlike processes increase with the increase in the projectile energy at above 10 MeV/A. It may be mentioned that, in the case of ICF reactions, the angular momentum associated is higher than the critical angular momentum of the system and indicates a possible way that may lead a composite system to fissionlike processes [14]. Nishio *et al.* [15] suggested the fission of an ICF composite nucleus as the dominant processes other than fission of the composite system formed by CF at intermediate energies. Furthermore, several authors [16–21] reported the existence of such reactions even at energies below 10 MeV/A, however, a survey on the literature displayed a considerable lack of experimental data to comment on the systematics of fissionlike processes.

It is notwithstanding to mention that the fission cross-sectional data in a variety of projectile and target combinations are important for understanding the formation of

*rakuiuac@gmail.com
†bpsinghamu@gmail.com

the superheavy elements in a laboratory [22], nuclear astrophysics [23], and, of course, nuclear energy [24]. One of the most important observations, in the low-energy fission of the actinides [25], was the discovery of asymmetric mass distribution and may be explained in terms of shell effects. A review [26] on this topic suggests that the gradual washing out of the shell effects at sufficiently higher excitation energies may lead to the disappearance of the asymmetric fission, and such fission mass distribution may follow the liquid-drop model. It may be pointed out that the charge and mass distributions are two indispensable postfission observables that are extensively studied at intermediate energies to understand the fading of shell effects with excitation energy and, in fact, in the development of the fission dynamics. Despite extensive work carried out for a wide range of fissility, excitation energy, and other entrance channel parameters [16,27–29], a complete understanding of the mechanism of various types of reactions populated at low energies and their dependence on a suitable set of physical parameters is still missing. Measurement of evaporation residues and the fission residues in a nuclear reaction may provide a comprehensive picture of the processes subsequent to the collision between the projectile and the target nuclei.

In view of the above, a program to study the dynamics of processes involved in the $^{14}\mathrm{N} + {}^{181}\mathrm{Ta}$ system has been undertaken. The independent (I) and cumulative (C) cross sections of several fissionlike products at $E_{\mathrm{lab}} = 82.2 \pm 0.8,\ 79.18 \pm 0.82,\ 76.8 \pm 1.2$, and 72.9 ± 0.91 MeV were measured and are reported in this paper. Furthermore, analysis has been performed to obtain the isotopic yield and mass distributions of residues populated via fission. The variances of the mass distribution have been determined in the present paper and are compared with the literature values to investigate the entrance channel effects on the onset of fission. The formation cross sections of ^{191}Hg, ^{190}Hg, ^{190}Au, ^{189}Pt, ^{188}Pt, ^{187}Pt, and ^{187}Ir evaporation residues (ERs) are analyzed within the framework of the PACE code [30]. It has been observed that the experimental cross section for the exit channels involving α particles are higher than PACE predictions which may be attributed due to the incomplete fusion reaction processes. An actual mass distribution of the total reaction residues reveals a wide mass distribution for the fission events whereas narrow mass distribution for the evaporation residues.

The present paper is organized as follows. The experimental details and methodology are given in Sec. II. The data reduction procedure, analysis, and results interpretation are given in Sec. III, whereas Sec. IV deals with the conclusions and summary of the present paper.

II. EXPERIMENTAL DETAILS AND METHODOLOGY

The experiments were performed using a $^{14}\mathrm{N}^{7+}$ beam obtained from the 15UD pelletron accelerator at the Inter-University Accelerator Centre (IUAC), New Delhi, India at projectile energies $E_{\mathrm{lab}} \approx 83$ and 80 MeV. To cover four energy points in an irradiation, an energy degradation technique was used. It may be mentioned that incident beam energy on each target foil in a stack was estimated using the code SRIM [31]. For example, at the highest incident

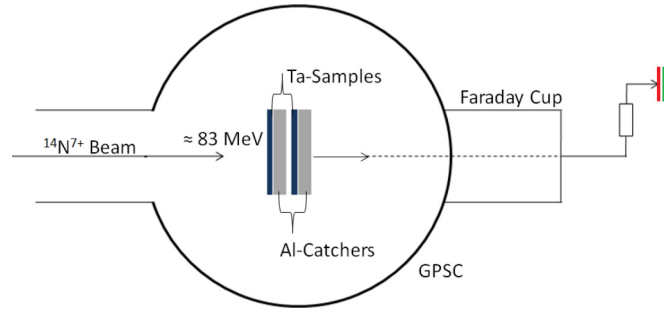

FIG. 1. Sketch of a typical experimental setup used for the irradiation.

energy the uncertainty in the energy due to finite sample thickness is estimated to be 0.80 MeV. The four studied energies are $82.2 \pm 0.8,\ 79.18 \pm 0.82,\ 76.8 \pm 1.2$, and 72.9 ± 0.91 MeV, respectively. The thin target foils of isotopically pure (≈99.9% purity) tantalum of thickness 1.3–1.9 mg/cm^2 were used for the irradiations. Aluminum catcher foils of sufficient thicknesses were used to collect the fission products and the evaporation residues recoiling out of the samples. The thicknesses of the Al catchers were chosen keeping in view the fact that even the most energetic residues produced as a result of complete momentum transfer may be trapped in the catcher thicknesses. It may be pointed out that recoil energy of the composite system (^{195}Hg) formed in $^{14}\mathrm{N} + {}^{181}\mathrm{Ta}$ as a result of complete momentum transfer from projectile to target at 82.20 ± 0.8 MeV is 5.90 MeV. The range of these 5.90-MeV heavy residues in Al is 303 μg/cm^2. As such, they are completely stopped in the catcher thickness used in the present paper. The ^{181}Ta foil samples and Al catchers were cut into 1.2×1.2-cm^2 size and pasted on Al holders having concentric holes of 1.0-cm diameter. Each target was followed by an Al catcher. The Al holders were used for the rapid dissipation of heat produced during the irradiation. The irradiations were carried out in the general purpose scattering chamber of 1.5-m diameter having an in-vacuum transfer facility. The beam current on the target was measured by a Faraday cup and was in the range of 20–25 pnA in both irradiations. A sketch of the typical experimental setup is shown in Fig. 1. Keeping in view the half-lives of interest, irradiations have been carried out for 10–12 h. The beam flux was monitored using an ORTEC current integrator by taking into account the charge collected in the Faraday cup, placed behind the stack of the target-catcher assembly. After the irradiation, activities induced in the target-catcher assembly were measured together employing a high efficiency high-purity germanium detector coupled to a CAMAC-based data-acquisition system. The absolute γ-ray detection efficiency of the detector was determined with an accuracy better than 5%. The resolution of the detector was 2.2 keV at 1408 keV. In the present paper, the standard γ sources and irradiated target-catcher foil assemblies were counted in the same geometry in order to avoid the errors due to the solid angle effect during the counting. The target-detector separation was suitably adjusted so as to keep the dead time <10%. In order to detect and follow the residues of shorter-longer half-lives, the counting of irradiated samples has been performed for a week or so.

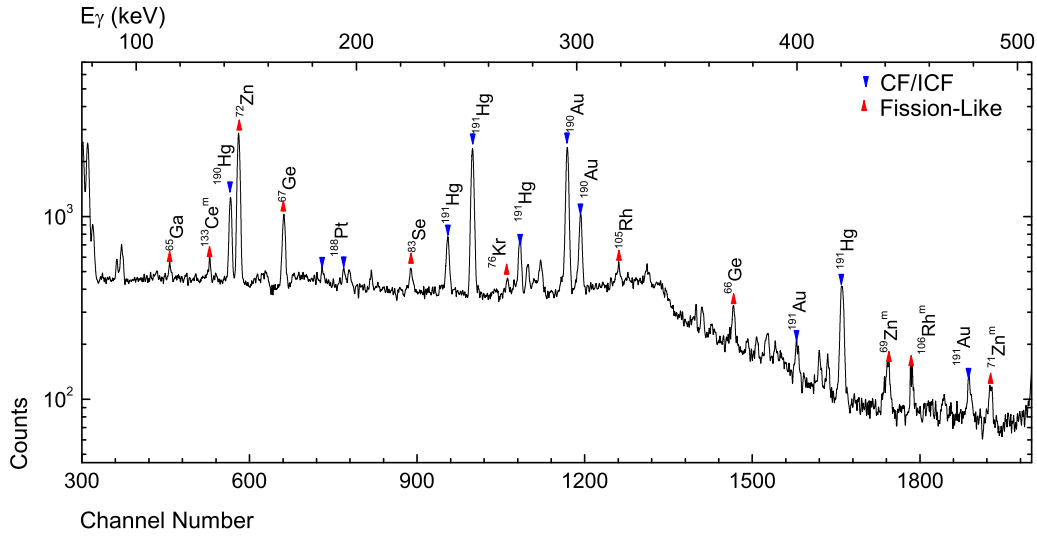

FIG. 2. Typical γ-ray spectrum of ^{14}N + ^{181}Ta interactions at $E_{lab} = 82.20 \pm 0.80$ MeV, where γ lines are assigned to the different reaction products expected to be populated via the CF, ICF, complete fusion-fission, and/or incomplete fusion-fission processes.

The γ spectra of the samples were recorded at increasing times, keeping in view that the decay curve required analysis for identification of reaction products. A typical γ-ray spectrum populated in 82.2 ± 0.8 MeV $^{14}N^{7+}$-induced reactions on ^{181}Ta is shown in Fig. 2. The γ peaks shown in Fig. 2 are assigned to fission (upward arrows) and evaporation residues (downward arrows) identified in the present paper. The γ-ray spectra were analyzed using a PC version of the CANDLE software [32]. The preliminary identification of reaction residues has been performed from their observed characteristic γ rays, which were further confirmed from their decay curve analysis. This is a very specific way to identify reaction products because each radioactive isotope has a unique half-life. Thus, the observed intensity of the identified γ ray is a measure of the production cross section of that particular reaction channel. Detailed analyses of experimental errors are given elsewhere [33]. The overall errors in the measured cross sections, including statistical errors, are estimated to be $\leqslant$15%.

III. DATA REDUCTION PROCEDURE, ANALYSIS, AND RESULTS INTERPRETATION

The evaporation residues and the fissionlike events populated have been measured using the stacked foil activation technique followed by an offline γ-ray spectroscopy. It may be emphasized that the activation technique is a nondestructive method of measuring the concentration of constituents in a given sample by measuring the characteristic radiations emitted by the radioactive nuclides resulting from the specific nuclear transformations. Although, the activation technique is quite simple and accurate, but sometimes it becomes complicated due to the presence of radiations (γ rays) of almost similar energies for more than one reaction product. In the case of mixing of nearby γ rays due to different isotopes, the contribution of each isotope can be separated out by decay curve analysis. It may, however, be pointed out that this technique is limited only for the reaction products having measurable half-lives. As a typical example, Fig. 3 shows the observed decay curves, respectively, for ^{65}Ga ($T_{1/2} = 15.2$ m) at 82.20 ± 0.80 MeV. The nuclear datalike half-lives, γ-ray energies, etc., have been taken from the Decay Radiation database via the NUDAT application [34]. The decay data of the reaction residues identified in the present paper are tabulated in Table I. In the case of fissionlike events, the independent and cumulative decay modes are marked by *I* and *C*, respectively. Furthermore, the intensities of the observed γ rays were used to calculate the formation cross section (σ_{exp}) for the reaction residues using the standard activation equation [33]. To have experimental cross sections for all the reaction residues identified in the present paper, initially we measured the experimental cross section of neutron emission channels viz., ^{191}Hg($4n$) and ^{190}Hg($5n$) at the studied energies and analyzed within the framework of PACE4 [30] prescriptions as presented in the next subsection.

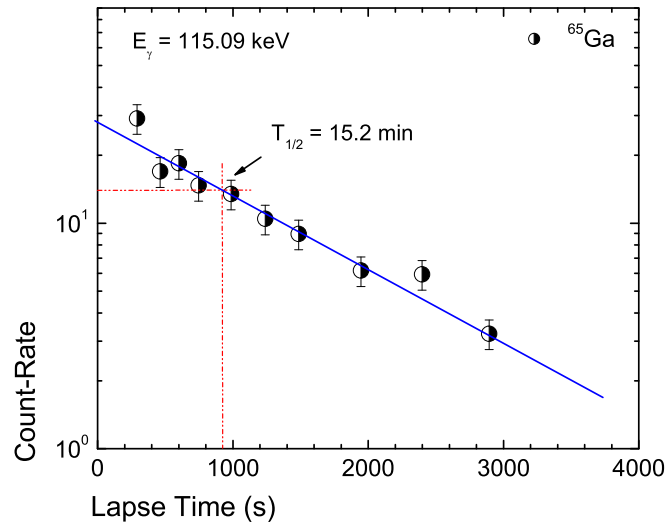

FIG. 3. A typical decay curve of gallium residue at obtained by following 115.01 keV γ-line.

TABLE I. Relevant nuclear data of the fission fragments and evaporation residues identified in the present paper.

S. No.	Nuclide	E_γ (keV)	γ-ray abundance I_γ (%)	Half-life	Decay mode
1	^{65}Ga	115.09	54.0	15.2 min	I
2	^{66}Ge	381.85, 272.97	28.3, 10.6	2.26 h	I
3	^{67}Ge	167.01	84.0	18.9 min	I
4	^{69}Ze^m	438.634	94.85	13.76 h	I
5	^{70}As	668.21, 905.61	21.1, 11.2	52.6 min	I
6	^{71}Zn^m	487.34, 620.19	61.2, 55.8	3.96 h	I
7	^{72}Ga	834.13	95.45	14.10 h	C
8	^{72}Zn	144.7	82.78	46.5 h	I
9	^{76}Kr	270.2	21	14.8 h	C
10	^{79}Kr	606.09	8.1	35.04 h	I
11	^{83}Se	225.22	29.5	22.5 min	I
12	^{95}Ru	626.83	17.8	1.64 h	C
13	^{105}Rh	318.9	19.1	35.36 h	I
14	^{106}In	632.66	91.8	10.2 min	I
15	^{106}Rh^m	450.8, 616.1	24.2, 20.2	131 min	I
16	^{108}In	1056.6	29	58.0 min	I
17	^{109}In	203.3	74.2	4.2 h	I
18	^{110}In	657.75	97.74	4.9 h	I
19	^{130}Sb	182.33	65	39.5 min	I
20	^{132}Ce	155.37	10.5	3.51 h	C
21	^{133}Ce^m	130.803	18.0	4.9 h	I
22	^{135}I	1038.76	7.9	6.57 h	C
23	^{191}Hg	252.6, 241.4	60, 12	50.8 min	$M1+E2, E2$
24	^{190}Hg	142.6,171.5	68, 4.8	20.0 min	$E1$
25	^{191}Au	399.84, 478.03	4.2, 3.5	3.18 h	$E2, M1+E2, E2$
26	^{190}Au	295.82, 301.82, 597.68	90, 29.7, 12.0	42.8 min	$E2$
27	^{188}Pt	187.59,195.05	19.4, 18.6	10.2 d	$M1+E2, M1$
28	^{187}Pt	201.52, 709.17	6.4, 5.2	2.35 h	$E1, M1$

A. Behavior of the evaporation residues in the framework of the PACE code

The experimental cross sections of residues ^{191}Hg ($4n$), ^{190}Hg ($5n$), ^{191}Au ($p3n$), and ^{190}Au ($p4n$) which are populated via $4n$, $5n$, $p3n$, and $p4n$ emissions, respectively, from the excited ^{195}Hg* CN have been measured at four different projectile energies viz., $E_{\rm lab} = 82.20 \pm 0.80$, 79.18 ± 0.82, 76.80 ± 1.20, and 72.94 ± 1.20 MeV and are compared with those estimated by statistical model code PACE4 [30]. It may be mentioned that the theoretical calculations were performed for a value of level density parameter $(a =)A/9$ MeV^{-1}. The ERs ^{191}Au and ^{190}Au are observed to have substantial feeding from their higher charge precursor isobars through electron capture and/or the β^+-decay process. Hence, the independent production experimental cross sections ($\sigma^{\rm ind}_{pxn}$) have been extracted from the cumulative experimental cross section ($\sigma^{\rm cum}_{pxn}$) using the formalism prescribed by Cavinato *et al.* [35], based on standard Batemann equations [36]. From the present ER analysis, a good agreement among $4n$, $5n$, $p3n$, and $p4n$ channel cross sections and PACE4 predictions are observed. For the sake of completeness, the ratio of experimentally measured and theoretically calculated cross sections of different evaporation residues identified at $E_{\rm lab} = 82.20 \pm 0.80$ MeV is shown in Fig. 4. As can be seen in this figure the ratio of experimentally measured and theoretically calculated production cross sections of ^{191}Hg, ^{190}Hg, ^{191}Au, and ^{190}Au follow the unity line. This clearly indicates the production of these residues via the complete fusion mode. However, the observed enhancement

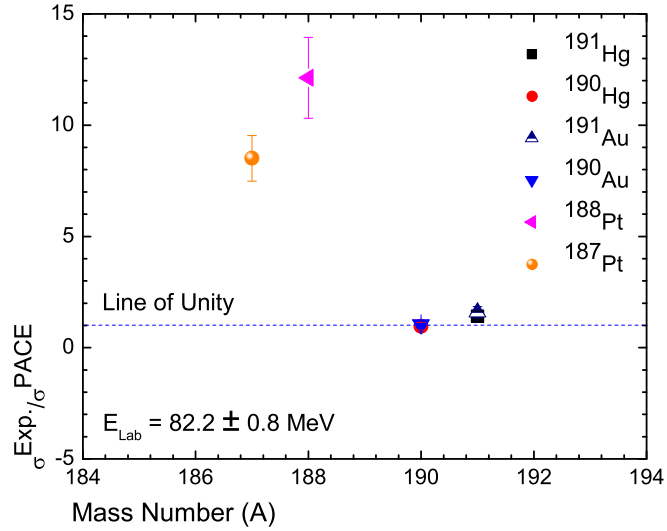

FIG. 4. Ratio of measured and PACE calculated cross sections of evaporation residues in the ^{14}N + ^{181}Ta reaction at $E_{\rm lab} = 82.20 \pm 0.80$ MeV. The dashed lines are drawn at unity.

TABLE II. Measured cross sections of the fission products formed in the $^{14}N + ^{181}Ta$ reaction at the studied projectile energies.

Nuclide	$E_{lab} = 82.2 \pm 0.8$ MeV σ (mb)	$E_{lab} = 79.18 \pm 0.82$ MeV σ (mb)	$E_{lab} = 76.8 \pm 1.2$ MeV σ (mb)	$E_{lab} = 72.9 \pm 0.91$ MeV σ (mb)
^{65}Ga	15.98 ± 2.39	9.89 ± 1.48	2.57 ± 0.38	
^{66}Ge	10.44 ± 1.56	5.17 ± 0.78		
^{67}Ge	38.25 ± 5.73	28.94 ± 4.34		
^{69}Zn^{m}	11.24 ± 1.68	8.20 ± 1.23	3.24 ± 0.48	
^{70}As	33.64 ± 5.04	27.44 ± 4.12	20.30 ± 3.04	
^{71}Zn^{m}	2.59 ± 0.38	5.43 ± 0.81	3.72 ± 0.56	1.25 ± 0.18
^{72}Ga	35.46 ± 5.32	26.04 ± 3.90	12.75 ± 1.92	2.37 ± 0.35
^{72}Zn	32.48 ± 4.87	19.90 ± 2.98	10.28 ± 1.54	
^{76}Kr	17.16 ± 2.57	16.13 ± 2.42		
^{79}Kr	28.21 ± 4.23	19.58 ± 2.93	15.24 ± 2.28	
^{83}Se	67.49 ± 10.12	51.97 ± 7.78	29.15 ± 4.37	16.16 ± 2.42
^{95}Ru	61.37 ± 9.20	56.21 ± 8.43	40.58 ± 6.08	20.12 ± 3.02
^{105}Rh	49.9 ± 7.48	50.31 ± 7.54	28.64 ± 4.29	28.53 ± 4.27
^{106}In	71.54 ± 10.73	55.81 ± 8.37	44.46 ± 6.67	15.48 ± 2.32
^{106}Rh^{m}	7.48 ± 1.16	10.25 ± 1.54		
^{108}In	92.20 ± 13.83	75.36 ± 11.30	61.21 ± 9.18	21.32 ± 3.19
^{109}In	74.68 ± 11.20	62.23 ± 9.33	30.19 ± 4.52	
^{110}In	38.03 ± 5.70	30.40 ± 4.56	9.23 ± 1.38	
^{130}Sb	42.50 ± 6.38	34.25 ± 5.14	17.89 ± 2.68	6.25 ± 0.93
^{132}Ce	28.50 ± 4.28	4.02 ± 0.60		
^{133}Ce^{m}	11.03 ± 1.65	7.17 ± 1.07	2.11 ± 0.32	1.49 ± 0.22
^{135}I	21.65 ± 3.24	17.49 ± 2.62	5.28 ± 0.79	1.26 ± 0.19

in the measured cross sections over the PACE4 values for ^{189}Pt ($\alpha 2n$), ^{188}Pt ($\alpha 3n$), ^{187}Pt ($\alpha 4n$), and ^{187}Ir ($\alpha p3n$) indicates their population via the projectile breakup process and may be attributed due to the ICF process. In Fig. 4, data for ^{188}Pt ($\alpha 3n$) and ^{187}Pt ($\alpha 4n$) are shown because for the ERs ^{189}Pt ($\alpha 2n$) and ^{182}Ir ($\alpha p3n$) PACE4 predicts negligible cross sections and the ratio of experimentally measured and theoretically calculated cross sections were not deduced. It may be mentioned that enhanced cross sections in the case for α-emitting channels may be a hint of the onset of ICF at this energy. Opting the same approach as that of xn, pxn, and αxn channels for measuring the experimental cross sections, the fissionlike events have been identified, and their cross sections are deduced and are discussed in the next section.

B. Assignment of fissionlike residues and their distributions

The unambiguous detection of 22 fissionlike fragments has been obtained first by their characteristic γ rays and then critically examined by their decay curve analysis. These residues are expected to be formed via: (a) the direct fission of the CF and/or ICF residues (i.e., first chance fission) and/or (b) by the fission of CF and/or ICF residues after emission of a few nucleons (second, third, etc., chance fission). On the other hand, the fission arises due to the decay of the excited composite system formed via complete momentum transfer from the projectile to the target nucleus [called complete fusion-fission (CFF)] and/or via incomplete momentum transfer from the projectile to the target nucleus [called incomplete fusion-fission (IFF)]. In the present paper, the yields of 17 fissionlike events are expected to be I as they are having no contribution from any precursor or shielded by stable or long-lived isotopes from their β^--decay chains. However, the isomeric yields of ^{69}Zn^{m}, ^{71}Zn^{m} ^{106}Rh^{m}, and ^{133}Ce^{m} represent the lower limit of the formation cross sections of ^{69}Zn, ^{71}Zn, ^{106}Rh, and ^{133}Ce. On the other hand, the yields of ^{72}Ga, ^{76}Kr, ^{95}Ru, ^{132}Ce, and ^{135}I have been found to be C as they have been fed by its precursors or populated from the β decay of the lower Z members of the fission product chains [37]. The measured cross sections for the identified fissionlike residues are tabulated in Table II at the studied projectile energies. In the present paper, fission isotopes were observed rather than the fission isobars; it is because of the fact that the emission of neutrons is more probable as compared to proton emission. Hence, a wide isotopic distribution of indium (^{106,108,109,110}In) is presented in the next subsection.

C. Isotopic yield distribution of indium

Analysis of isotopic distribution provides an access to one of the major characteristics of low-energy fission [38] and is a key observable for the modeling of the fission process. For the heavy composite systems at moderate excitation energies, the nucleon emission competes directly with fission. For such reaction processes, the emission of charged particles is severely hindered because of the large Coulomb barrier and nucleon emission from the fission fragments and/or the fission leading to successive elements of fission chains may give rise to the isotopic and isobaric distributions of the fission residues. Furthermore, it has been well known that the independent isotopic yields are well represented by a Gaussian distribution [42], therefore, the experimentally measured independent cross section of indium isotopes (^{106,108,109,110}In) are fitted

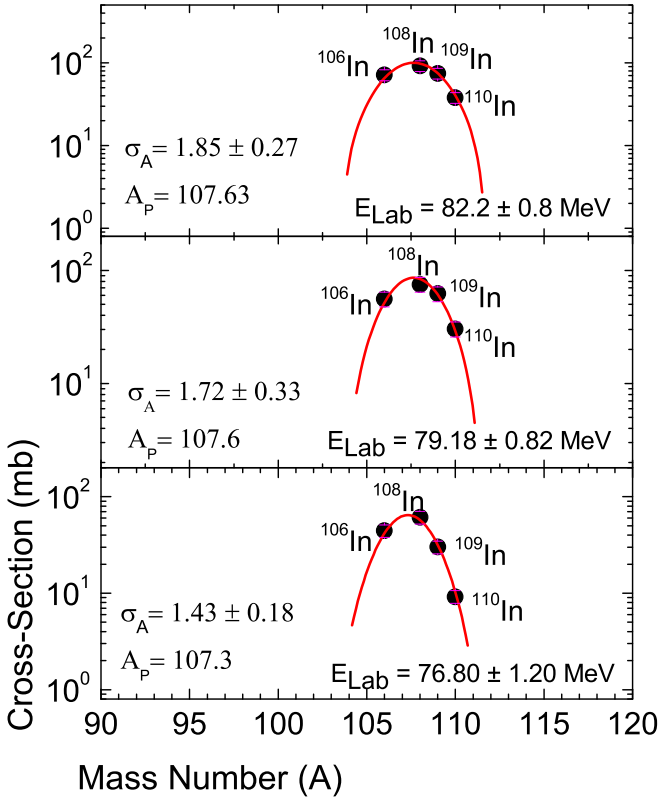

FIG. 5. Isotopic yield distribution for (^{106,108,109,110}In) indium isotopes in the ^{14}N + ^{181}Ta reaction.

with the Gaussian distribution,

$$Y(A) = \frac{Y_Z}{\sqrt{2\pi\sigma_A^2}} e^{-(A-A_p)^2/2\sigma_A^2}, \quad (1)$$

where $Y(A)$ is the independent yield of the indium isotopes and Y_Z is the chain yield of the indium isotopes. In Eq. (1), the parameters viz., A_P and σ_A^2 are the most probable mass and the variance obtained after the Gaussian fit (see Fig. 5), and the values are tabulated in Table III. It may be mentioned that the value of χ^2 was minimized using a nonlinear least-squares fit routine using ORIGIN software. For the identified indium isotopes, the most probable mass A_P and σ_A^2 compare well with the corresponding values of 108.42, and 4.16 ± 0.01 for ^{16}O + ^{181}Ta [39] at 100 MeV and 107.88 and 4.24 reported for the ^{16}O + ^{169}Tm system at 95 MeV [2].

Furthermore, the σ_A^2 values determined in the present paper are compared with the available literature values and are tabulated in Table IV. As can be seen from the table, the σ_A^2

TABLE III. Width (σ_A) of isotopic yield distribution for observed fission residues (indium) in the ^{14}N + ^{181}Ta system.

Excitation energy E^* (MeV)	Most probable mass A_P	Isotopic width $2\sigma_A$
61.72	107.6 ± 0.05	3.70 ± 0.27
58.92	107.6 ± 0.06	3.44 ± 0.33
56.70	107.3 ± 0.05	2.86 ± 0.18

TABLE IV. Comparison of isotopic yield distributions (σ_A^2) for different fissioning systems.

System	E^* (MeV)	Element	σ_A^2	References
^{14}N + ^{181}Ta	61.72	In	3.42 ± 0.54	[a]
^{14}N + ^{181}Ta	58.92	In	2.96 ± 0.66	[a]
^{14}N + ^{181}Ta	56.66	In	2.05 ± 0.36	[a]
^{16}O + ^{159}Tb	57.1	Sr	3.31	[2]
^{16}O + ^{159}Tb	57.1	Y	4.41	[2]
^{16}O + ^{169}Tm	61.06	In	4.24	[2]
^{16}O + ^{169}Tm	61.06	Tc	4.62	[2]
^{16}O + ^{181}Ta	67.041	Y	3.05 ± 0.10	[39]
^{16}O + ^{181}Ta	67.041	In	4.16 ± 0.01	[39]
^{7}Li + ^{232}Th	41.7	Sb	4.08	[40]
^{7}Li + ^{232}Th	41.7	I	3.96	[40]
^{11}B + ^{232}Th	55.7	Sb	4.0	[43]
^{11}B + ^{232}Th	55.7	I	5.43	[43]
^{11}B + ^{232}Th	55.7	Cs	3.72	[43]
^{11}B + ^{238}U	67.4	Rb	3.84 ± 0.16	[41]
^{11}B + ^{238}U	67.4	Cs	3.95 ± 0.14	[41]
^{22}Ne + ^{238}U	64.5	Rb	4.23 ± 0.40	[41]
^{22}Ne + ^{238}U	64.5	Cs	4.26 ± 0.90	[41]
^{20}Ne + ^{208}Pb	46.4	Sb	3.43 ± 1.02	[44]
^{20}Ne + ^{208}Pb	46.4	I	3.95 ± 0.87	[44]

[a]The present paper.

values are close to the literature values and give confidence to the present observations. It may be pointed out that a Gaussian distribution for indium isotopic distribution has been observed at excitation energies of 61.72, 58.92 and 56.66 MeV, however, at the lower incident energy (i.e., 72.94 ± 1.2 MeV) only a few isotopes were identified as expected, and therefore, their distribution could not be studied. Furthermore, using the prescriptions of Gubbi *et al.* [43], the isobaric charge dispersion parameters were obtained from the measured isotopic mass distribution. The fractional isotopic independent yields FY^I (Z) were obtained by dividing the independent yields by their corresponding charge yield. For deducing the total yield of mass A it is required to have knowledge of the isobaric charge dispersion parameter σ_Z and the most probable charge Z_p. The Z_p for the indium isotopes is calculated using

$$Z_p(A) = \frac{Z}{A_p} A, \quad (2)$$

where Z and A are the atomic number and the atomic mass number of indium fragments, respectively. The distribution of fractional chain yield vs the charge corrected isotopic fragments (Z-Z_P) so determined is shown in Fig. 6. The solid curve of Fig. 6 is the Gaussian fit.

The estimated isobaric charge dispersion parameter σ_Z from the Gaussian fitting procedure has been found to be 0.77 ± 0.10, 0.72 ± 0.06, and 0.59 ± 0.07 charge units at excitation energies ≈61.72, 58.92, and 56.66 MeV, respectively. The values of σ_Z have also been calculated by converting the width parameter of isotopic yield σ_A into σ_Z using

$$\sigma_Z = \frac{\sigma_A \times Z}{A_p}. \quad (3)$$

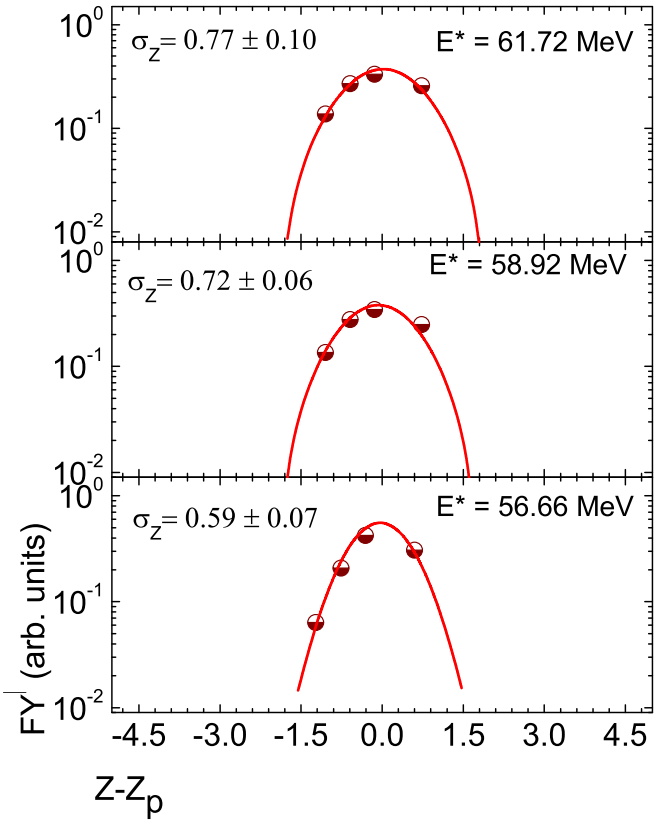

FIG. 6. Fractional isotopic yield corresponding to corrected charge distribution.

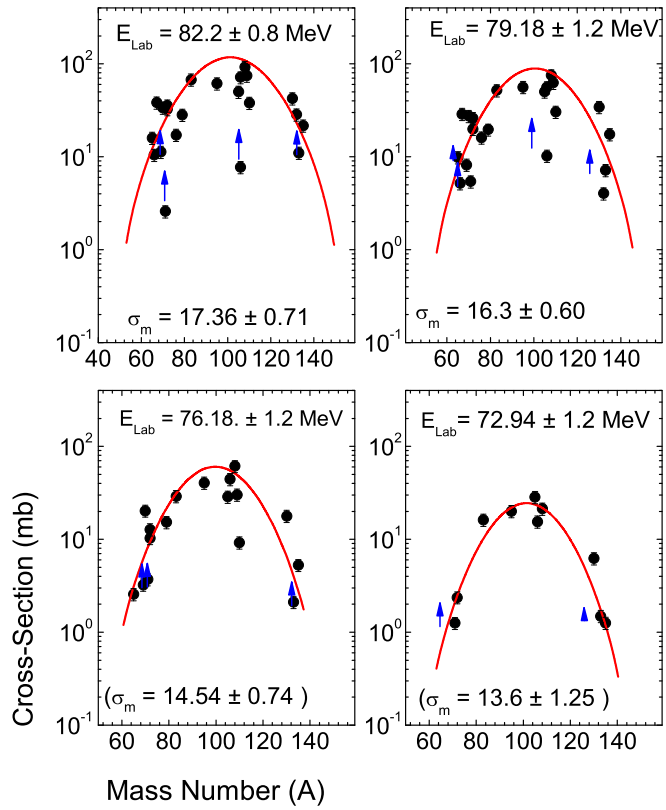

FIG. 7. Mass distribution of fission products in the $^{14}N + ^{181}Ta$ reaction at the studied energies. Upward arrows indicate values expected to go up. The lines are drawn through the data points for the Gaussian fit.

The calculated average value of width parameter σ_Z along with the value obtained for the corrected charge distribution (see Fig. 6) are found in good agreement, and the values are tabulated in Table V. The above method indicates self-consistency of the present analysis.

D. Mass distribution of fissionlike events

Fragments mass distribution is an important observable in fission which directly provide information related to the collective dynamics of the fission process [45,46]. In the present paper, activities measured in the forward catcher foils were used for the mass distribution studies. The plots of experimentally determined production cross sections (given in Table II) of various fission fragments at the studied energies (i.e., $E_{\rm lab} \approx 82.2 \pm 0.8$, 79.18 ± 0.82, 76.8 ± 1.2, and 72.9 ± 0.91 MeV) are shown in Fig. 7. The upward arrows indicate that only the metastable states have been measured, and the total production cross sections of these fission fragments are expected to get enhanced. As can be seen in Fig. 7, the mass distributions are found to be symmetric and can be fitted with one Gaussian function, indicating the formation of identified fissionlike fragments from the decay of the compound nucleus. It may be because of the fact that the mass flow from the projectile to the target in the initial dinucleus, i.e., a system with the mass asymmetry $(\alpha = M_T - M_P/M_T + M_P$, where M_T is the mass of the target nuclei and M_P is the mass of the projectile nuclei) greater than the critical mass asymmetry (α_{BG}), the system establishes a mononuclear compact shape which facilitates equilibrium in all degrees of freedom and thus fission proceeds via compound nuclear processes. In the present paper, the mass asymmetry (α) for the presently studied system is 0.856 and is found to be greater than the critical mass asymmetry $(\alpha_{BG} = 0.827)$ of the system which suggests that for fissionlike events the mass distribution is expected to be broad and symmetric. In order to track the change in mass variance (σ_M^2) with excitation energy, the value of σ_M obtained from the Gaussian fitting procedure of mass distributions of fissionlike fragments is plotted as a function of excitation energy in Fig. 8. As can be seen in Fig. 8, the value of σ_M^2 increases with excitation energy, indicating larger spread in fission-fragment masses for higher excitation energies. The observed variation in the value of σ_M^2 with

TABLE V. The isobaric charge dispersion parameter obtained after the Gaussian fit (see Fig. 6) and the same parameter has been calculated using Eq. (3).

Excitation energy E^* (MeV)	σ_Z From Fig. 6	σ_Z Using Eq. (3)
61.72	0.77 ± 0.10	0.84
58.92	0.72 ± 0.06	0.78
56.70	0.59 ± 0.07	0.65

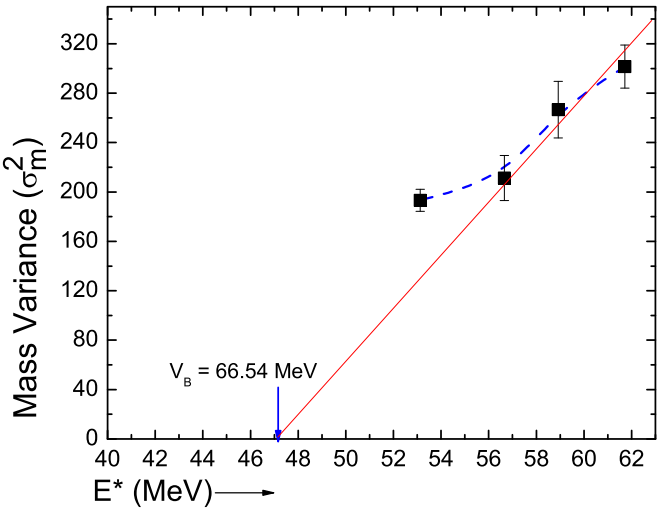

FIG. 8. Mass variance as a function of excitation energy for ^{195}Hg. The solid lines show the increase in σ^2 with E^*. The vertical arrow indicates the excitation energy corresponding to the Coulomb barrier.

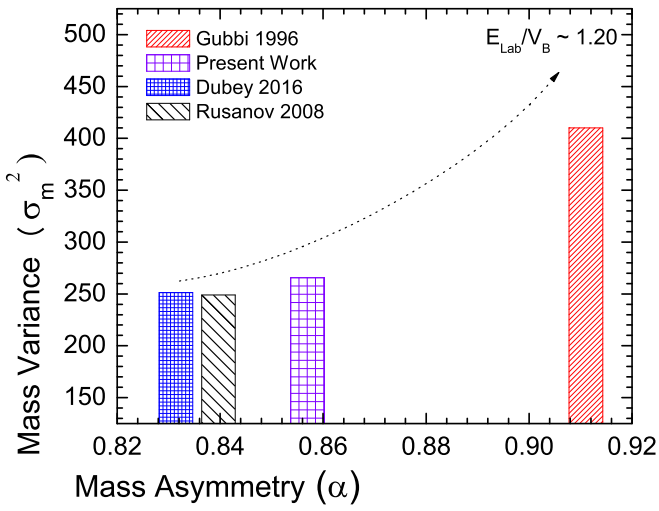

FIG. 9. Mass asymmetry vs variances for the three projectile-target combinations (Gubbi *et al.* 1996 [43], Dubey *et al.* 2016 [50], Rusanov *et al.* 2008 [51]).

excitation energy for the present system follows the same trend as that reported by Ghosh *et al.* [47] in the above-barrier region for three different projectiles (^{19}F, ^{16}O, and ^{12}C) on a deformed target (^{232}Th). It may be mentioned that the present system was studied at only four energies above the barrier, hence the variation of the value of σ_M^2 with excitation energy at and below the barrier energies needs to be further investigated to better understand this aspect.

Furthermore, the stability (stiffness) of the fissioning nucleus to mass-asymmetric deformation can be understood through observed mass distribution. To understand this aspect, Itkis *et al.* [48] and Rusanov *et al.* [49] analyzed a large collection of data over a wide range of fissility of the compound nucleus at medium excitation energies. In the present paper, the calculated centroid, width, and variance of the mass distribution obtained were compared with the values reported in the literature for similar systems. As such, the fission of ^{195}Hg mass distributions reported in Ref. [52] for the ^{13}C + ^{182}W reaction indicates the symmetric mass division. The calculations by Itkis *et al.* [53] indicate the symmetric mass distribution for the ^{198}Hg isotope. On the other hand, for lower mass isotopes of Hg (i.e., ^{180,184}Hg) the experimental mass distributions are found to be asymmetric [54]. Similar asymmetric distributions were observed for the Hg isotopes ranging $^{180–188}$Hg [55]. Hence, it may be concluded from the mass distribution of Hg isotopes, in particular the heavier ones (i.e., $^{x>195}$Hg), that the strong shell effects plays an important role for the symmetric mass distribution, and the shape of the mass distribution may be defined by the liquid-drop part of the energy.

In order to understand the role of the entrance channel parameter on the behavior of mass distribution of fissionlike fragments, the available mass variance of the fission fragments for different projectile-target combinations were compared with the presently calculated mass variance as a function of mass asymmetry (α). Figure 9 shows the distribution of the variance with respect to α for four projectile-target combinations at constant projectile energy normalized with the Coulomb barrier (V_B). From the figure, it is noted that the mass variance increases with the mass asymmetry (α) of the interacting ions. This suggests a broader distribution of fission fragments for the more mass asymmetric system. However, more projectile-target combinations with different mass asymmetry values are needed to understand the dependence of mass variance on α. Furthermore, an attempt has been made to visualize the actual picture of the total mass distribution of the residues (fissionlike events + evaporation) and is plotted in Fig. 10 at $E_{lab} = 82.2 \pm 0.80$ MeV. As can be seen in the figure, the peak at higher mass number may be attributed to

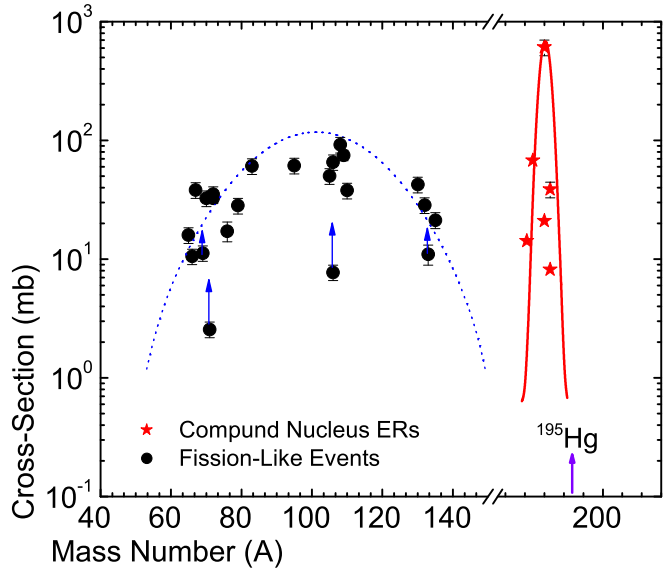

FIG. 10. Schematic of fission fragments and compound nucleus evaporation residues at $E_{lab} = 82.20 \pm 0.80$ MeV. The solid lines are drawn through the data points to guide the eyes.

the residues formed by light particle evaporation, whereas the broad peak in the intermediate mass region may be assigned to fissionlike events. This may be because of the fact that the prescission emission of light-charged particles dominate close to the Coulomb barrier due to dynamical hindrance to fission and can strongly affect the observed mass distributions of those events that succeed to fission [56,57].

IV. SUMMARY AND CONCLUSIONS

In the present paper, several fission fragments populated via CFF and/or IFF processes in the $^{14}N + ^{181}Ta$ system at $E_{lab} = 82.2 \pm 0.8,\ 79.18 \pm 0.82,\ 76.8 \pm 1.2$, and 72.9 ± 0.91 MeV have been identified, and their production cross sections have been obtained. The data have been analyzed to deduce parameters of isotopic yield distribution. The isotopic yield distributions are satisfactorily reproduced by single Gaussian distribution. The distribution parameters obtained from the present measurements agree reasonably well with the literature values. The mass distribution of fission fragments at different excitation energies was studied to probe the behavior of fission fragments. The mass distribution of fissionlike events was found to be symmetric at all the studied energies and can be fitted with one Gaussian function, indicating the population of fission fragments via deexcitation of the compound nucleus. The behavior of the measured mass variance is studied in terms of excitation energies. Furthermore, the mass variance is studied with respect to mass asymmetry at constant normalized projectile energies. It has been observed that mass variance exponentially increases with mass asymmetry of the system. However, more experiments are required for the different projectile and target combinations to explore the actual picture of the mass asymmetry systematics. An online experiment employing the fission detectors by measuring the neutron multiplicity using the neutron array setup is proposed to get a detailed insight into fission dynamics for the system.

ACKNOWLEDGMENTS

The authors thank the Director of the IUAC, New Delhi, India for extending experimental facilities. V.R.S. and E.F.A. thank CONACYT for providing financial support under Project No. CB-01-254619. M.S., B.P.S., and R.P. thank the DST-SERB Project No. EMR/2016/002254 for financial assistance.

[1] L. G. Moretto, D. Heuneman, R. C. Jared, R. C. Gatti, and S. G. Thompson, *Physics and Chemistry of Fission* (Intern. Atomic Energy Agency, Vienna, 1974), Vol. II, p. 351.
[2] P. P. Singh, B. P. Singh, B. Sharma, Unnati, M. K. Sharma, R. Prasad, R. Kumar, and H. D. Bhardwaj, Int. J. Mod. Phys. E **17**, 549 (2008).
[3] W. Udo Schröder, Pramana **85**, 227 (2015).
[4] D. J. Hinde *et al.*, J. Phys.: Conf. Ser. **420**, 012115 (2013).
[5] W. Gawlikowicz *et al.*, Phys. Rev. C **81**, 014604 (2010).
[6] M. Dasgupta, D. J. Hinde, R. D. Butt, R. M. Anjos, A. C. Berriman, N. Carlin, P. R. S. Gomes, C. R. Morton, J. O. Newton, A. Szanto de Toledo, and K. Hagino, Phys. Rev. Lett. **82**, 1395 (1999).
[7] E. F. Aguilera *et al.*, Phys. Rev. Lett. **107**, 092701 (2011).
[8] H. C. Britt and A. R. Quinton, Phys. Rev. **124**, 877 (1961).
[9] F. Hanappe, M. Lefort, C. Ngo *et al.*, Phys. Rev. Lett. **32**, 738 (1974).
[10] V. E. Viola, K. Kwiatkowski, and M. Walker, Phys. Rev. C **31**, 1550 (1985).
[11] K.-H. Schmidt and B. Jurado, Phys. Rev. Lett. **104**, 212501 (2010).
[12] T. Sikkeland, E. L. Haines, and V. E. Viola, Jr., Phys. Rev. **125**, 1350 (1962).
[13] V. E. Viola, Jr., B. B. Back, K. L. Wolf, T. C. Awes, C. K. Gelbke, and H. Breuer, Phys. Rev. C **26**, 178 (1982).
[14] A. Pal *et al.*, Phys. Rev. C **98**, 031601(R) (2018).
[15] K. Nishio, H. Ikezoe, Y. Nagame, M. Asai, K. Tsukada, S. Mitsuoka, K. Tsuruta, K. Satou, C. J. Lin, and T. Ohsawa, Phys. Rev. Lett. **93**, 162701 (2004).
[16] J. V. Kratz, J. O. Liljenzin, A. E. Norris, and G. T. Seaborg, Phys. Rev. C **13**, 2347 (1976).
[17] D. J. Hinde, J. R. Leigh, J. J. M. Bokhorst, and J. O. Newton, Nucl. Phys. A **472**, 318 (1987).
[18] J. P. Lestone, J. R. Leigh, J. O. Newton, and J. X. Wei, Nucl. Phys. A **509**, 178 (1990).
[19] M. C. Duh, H. Baba, N. Takashi, A. Yokoyama, and T. Saito, Nucl. Phys. A **550**, 281 (1992).
[20] A. Pagano, S. Aiello, E. De Filippo, G. Lanzano, S. Lo Nigro, C. Milone, G. Blancato, G. Di Marco, and M. C. Mermaz, Phys. Rev. C **47**, 1170 (1993).
[21] G. K. Gubbi, A. Goswami, B. S. Tomar, B. John, A. Ramaswami, A. V. R. Reddy, P. P. Burte, and S. B. Manohar, Phys. Rev. C **53**, 796 (1996).
[22] H. C. Manjunath and K. N. Sridhar, Nucl. Phys. A **962**, 7 (2017).
[23] B. B. Back, J. A. Clark, R. C. Pardo, K. E. Rehm, and G. Savard, AIP Adv. **4**, 041005 (2014).
[24] L. S. Leong, Fission fragment angular distribution and fission cross section validation, Thesis Doctoral, University Paris Sud-Paris XI, 2013.
[25] R. Tripathi and A. Goswami, Eur. Phys. J. A **26**, 271 (2005).
[26] A. N. Andreyev, K. Nishio, and K.-H. Schmidt, Rep. Prog. Phys. **81**, 016301 (2018).
[27] C. Ngô, Prog. Part. Nucl. Phys. **16**, 139 (1985).
[28] J. R. D. Todd, A. R. Wolf, J. J. Hogan, and D. J. Parker, J. Phys. G **19**, 187 (1993).
[29] V. S. Ramamurthy, S. S. Kapoor, R. K. Choudhury, A. Saxena, D. M. Nadkarni, A. K. Mohanty, B. K. Nayak, S. V. Sastry, S. Kailas, A. Chatterjee, P. Singh, and A. Navin, Phys. Rev. Lett. **65**, 25 (1990).
[30] O. B. Tarasov and D. Bazin, Nucl. Instrum. Methods Phys. Res., Sect. B **204**, 174 (2003).
[31] SRIM06; http://www.srim.org /
[32] R. Kumar *et al.*, Proc. DAE-BRNS Symp. Nucl. Phys. B **52**, 647 (2007); S. Venkataramanan *et al.*, *ibid.* **45**, 424 (2002); E. T. Subramaniam *et al.*, Rev. Sci. Instr. **77**, 096102 (2006).

[33] V. R. Sharma, M. Phil. Dissertation-Published, A. M. University, India (2011), http://ir.amu.ac.in/7693/.
[34] Decay Radiation database version of 01−03−2018 http://www.nndc.bnl.gov/nudat2/.
[35] M. Cavinato, E. Fabrici, E. Gadioli, E. Gadioli Erba, P. Vergani, M. Crippa, G. Colombo, I. Redaelli, and M. Ripamonti, Phys. Rev. C **52**, 2577 (1995).
[36] R. D. Evans, *The Atomic Nucleus* (McGraw-Hill, New York, 1995).
[37] J. A. McHugh, Jr, Thesis Doctoral, University of California.
[38] C. Donzaud *et al.*, Eur. Phys. J. A **1**, 407 (1998).
[39] V. R. Sharma, A. Yadav, P. P. Singh, M. K. Sharma, D. P. Singh, Unnati, R. Kumar, K. S. Golda, B. P. Singh, A. K. Sinha, and R. Prasad, Phys. Rev. C **84**, 014612 (2011).
[40] R. Tripathi, K. Sudarshan, S. Sodaye, B. S. Tomar, G. K. Gubbi, A. Goswami, A. V. R. Reddy, and S. B. Manohar, Radiochem. Acta **90**, 185 (2002).
[41] M. de Saint-Simon *et al.*, Phys. Rev. C **14**, 2185 (1976).
[42] J. H. Hamilton *et al.*, Prog. Nucl. Part. Phys. **35**, 635 (1995); Phys. Rep. **264**, 215 (1996).
[43] G. K. Gubbi, A. Goswami, B. S. Tomar, A. Ramaswami, A. V. R. Reddy, P. P. Burte, S. B. Manohar, and B. John, Phys. Rev. C **59**, 3224 (1999).
[44] R. Tripathi, K. Sudarshan, A. Goswami, P. K. Pujari, B. S. Tomar, and S. B. Manohar, Phys. Rev. C **69**, 024613 (2004).
[45] A. C. Berriman, D. J. Hinde, M. Dasgupta, C. R. Morton, R. D. Butt, and J. O. Newton, Nature (London) **413**, 144 (2001).
[46] D. J. Hinde, A. C. Berriman, R. D. Butt, M. Dasgupta, I. I. Gontcher, C. R. Morton, A. Mukherjee, and J. O. Newton, J. Nucl. Radiochem. Sci. **3**, 31 (2002).
[47] T. K. Ghosh *et al.*, Phys. Lett. B **627**, 26 (2005).
[48] M. G. Itkis, Y. A. Muzychka, Y. T. Oganessian, V. N. Okolovich, V. V. Pashkevich, A. Y. Rusanov, V. S. Salamatin, G. N. Smirenkin, and G. G. Chubarian, Phys. At. Nucl. **58**, 2026 (1995).
[49] A. Y. Rusanov, M. G. Itkis, and V. N. Okolovich, Phys. At. Nucl. **60**, 683 (1997).
[50] R. Dubey *et al.*, Phys. Lett. B **752**, 338 (2016).
[51] A. Y. Rusanov *et al.*, Phys. At. Nucl. **71**, 956 (2008).
[52] E. Prasad, D. J. Hinde, E. Williams *et al.*, EPJ Web Conf. **123**, 03006 (2016).
[53] M. G. Itkis, V. N. Okolovich, and G. N. Smirenkin, Nucl. Phys. A **502**, 243c (1989).
[54] A. V. Andreev, G. G. Adamian, and N. V. Antonenko, Phys. Rev. C **86**, 044315 (2012).
[55] P. Moller, J. Randrup, and A. J. Sierk, Phys. Rev. C **85**, 024306 (2012).
[56] D. Jacquet and M. Morjean, Prog. Part. Nucl. Phys. **63**, 155 (2009).
[57] J. O. Newton, Pramana **33**, 175 (1989), and references therein.